Investigating Taconis oscillations in a U-shaped tube with hydrogen and helium

Authors: Matthew P. Shenton, Jacob W. Leachman, and Konstantin I. Matveev¹

Hydrogen Properties for Energy Research (HYPER) Center, School of Mechanical and Materials Engineering, Washington State University, Pullman, WA 99164, USA

Abstract

Taconis oscillations are thermally induced spontaneous excitations of acoustic modes in tubes subjected to large temperature gradients. Cryogenic systems that experience these excitations suffer from increased heat leak and vibrations. This heat leak may also increase boil-off in longterm storage vessels for liquid hydrogen. In this study, U-shaped closed-end tubes with a cold mid-section are experimentally investigated to quantify the oscillation characteristics for hydrogen- and helium-filled systems at various mean pressures, including supercritical hydrogen states. Experimental measurements of the temperature distribution along the tube and acoustic pressure amplitudes and frequencies are taken in constant- and variable-diameter configurations near the onset of oscillations. Thirty different conditions are recorded with mean pressures ranging from 126 kPa to 1127 kPa for helium and 161 kPa to 1816 kPa for hydrogen. A lowamplitude thermoacoustic model is applied to predict the cold temperature and frequency corresponding to the onset of Taconis oscillations. The findings of this study indicate that Taconis oscillations in systems with hydrogen occur at smaller temperature differences than in more traditional helium systems by approximately 10 K. Hydrogen in the constant-diameter configuration excited when cryogenic temperatures reached 35-40 K, whereas helium excited when cryogenic temperatures reached 20-30 K. Special tubing networks, such as wider segments in the warm portion, can drastically elevate the excitation cold temperature resulting in onset temperatures between 50-60 K for both fluids. Taconis oscillations are also found to exist in conditions when liquid hydrogen starts forming in the cold zone of the system, as well as in supercritical states. The presented measurements are useful for designing cryogenic hydrogen storage systems to control these oscillations.

Keywords: Taconis oscillations, thermoacoustics, cryogenic instabilities, liquid hydrogen.

1

¹ Corresponding author. E-mail: matveev@wsu.edu

1. Introduction

Thermoacoustic oscillations are often defined as sound waves that spontaneously appear due to thermal instabilities of acoustic modes inside conduits with large temperature gradients. The occurrence of these oscillations can be associated with the Raleigh thermoacoustic criterion [1] which states that acoustic motion is encouraged if heat is added to the fluid when the fluid is compressed and heat is removed when the fluid is rarified. Sound is generated when this conversion of thermal-to-acoustic energy exceeds acoustic dissipative losses in the system. In 1949, Taconis et al. discovered these oscillations in a cryogenic setup [2]. They encountered thermoacoustic instabilities inside a tube inserted into a liquid helium dewar while measuring vapor-liquid equilibrium of helium-3 and helium-4 mixtures. In the classical Taconis setting, the end of the tube outside of the dewar is closed, and the end inside of the dewar is open, as shown in Figure 1a. Parameters T_h and T_c are defined as the hot temperature in the ambient environment and the cold temperature in the cryogenic environment, respectively.

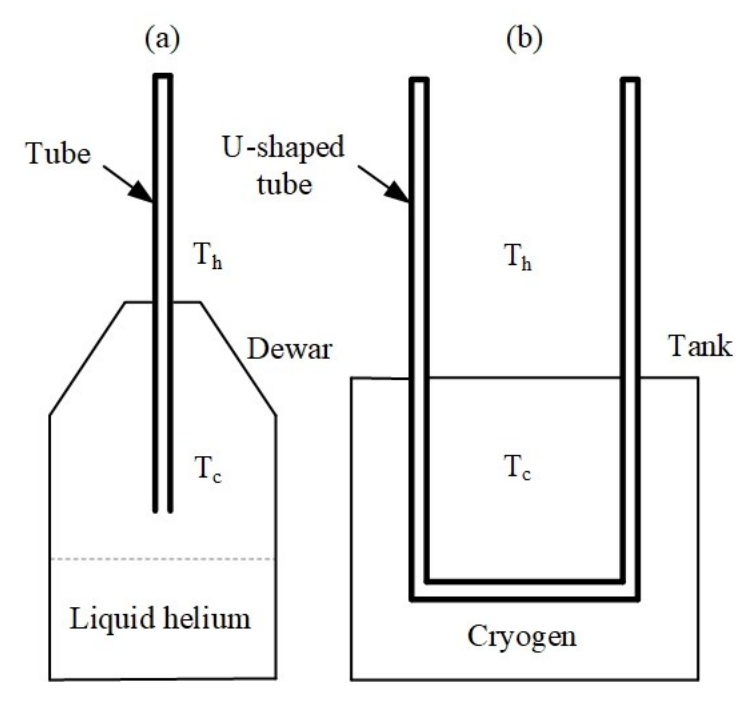


Figure 1. (a) Classic Taconis setup with a tube inserted into a liquid helium dewar. (b) U-shaped tube immersed in a cryogenic fluid tank.

Different analytical and numerical approaches have been applied for modeling this process and experimental studies have been conducted to quantify these oscillations. A summary of the major studies conducted on Taconis oscillations is presented below and listed in Table 1.

Rott [3] established fundamental equations to characterize thermal oscillations for the acoustic waves in a tube by re-examining the assumptions of earlier work by Kramers [4] (that did not produce good agreement with test data). Rott used a low-amplitude approach, without the boundary layer approximation, to obtain realistic temperature ratios for the excitation of oscillations in real systems. Later, Rott [5] used these equations to calculate the stability limits for helium in a classical setup (Figure 1a). Von Hoffmann et al. [6] experimentally verified Rott's findings by measuring the stability limit for cryogenic helium. Rott [7] continued work

characterizing the stability limits with helium and nitrogen in tubes with variable cross sections, and with Zouzoulas [8] discussed the stability limits for gas-liquid oscillations with helium and nitrogen. Swift et al. [9] expanded Rott's theory to account for additional elements in thermoacoustic systems; enabling a broader range of operational conditions and phenomena useful for the practical design of thermoacoustic engines and refrigerators, including cryocoolers. The modeling performed in the present work is based on theories from Rott's and Swift's works.

Dmitrevskiy et al. [10] and Yazaki et al. [11] obtained experimental measurements for Taconis oscillations. Dmitrevskiy et al. [10] quantified the effect on oscillations of variable depth of a tube immersed into the liquid in a classical setup encompassing different working fluids, including nitrogen, argon, oxygen, and hydrogen. Yazaki et al. [11] employed a symmetric setup (Figure 1b), with cryogenic temperatures in the middle of the tube and compared the experimental measurements to the stability limits for helium. Their measurements showed agreement with Rott's thermoacoustic equations defining the stability limits for helium. A study by Spradley et al. [12] aimed to investigate boil-off rates due to heat leak associated with these oscillations in liquid hydrogen storage vessels aboard space vehicles. However, helium was substituted for hydrogen due to safety considerations. They utilized the classical setup, shown in Figure 1a. They found that the heat leak can be at least two orders of magnitude higher than normal conduction into the system which limits the storage life of cryogens, but no predictions about hydrogen boil-off were discussed. A recent study by Christie et al. [13] revisited Taconis oscillation research for ground storage vessels using mitigation techniques described by Putselyk et al. [14] and Luck et al. [15].

This present work is motivated by the rising importance of liquid hydrogen fuel as a clean and renewable energy carrier. Long-term storage solutions are imperative for broader applications of liquid hydrogen. Taconis oscillations can be present in the tubing penetrating the storage vessels due to large temperature differences between ambient surroundings and the cryogenic conditions inside tanks. The convective heat transfer due to oscillatory flow associated with Taconis phenomenon can increase parasitic heat leak which can go unaccounted for, as conventional pressure gauges may not resolve the oscillations as mentioned by Keller [16]. With few experimental datasets available for Taconis effects in hydrogen systems, the current study aims to provide detailed measurements and apply thermoacoustic theory to determine the stability limits for Taconis oscillations in hydrogen setups. A new cryostat has been developed to test different geometric configurations and characterize Taconis oscillations in cryogenic fluids [17]. The experimental apparatus (detailed in Section 2) uses a U-shaped tube related to the symmetric configuration described by Yazaki [11]. Experimental data is obtained utilizing both helium and hydrogen to compare onset parameters between fluids as previous studies have primarily performed measurements and numerical calculations for helium. The onset characteristics of the experimental configurations are calculated from the thermoacoustic model described in Section 3. Comparisons between the thermoacoustic theory, the obtained experimental measurements, and the two cryogenic fluids are presented in Section 4.

Table 1. Summary of previous literature on Taconis oscillations.

Author	Method	Setup	Working fluid	Outcomes
Taconis et al. [2]	Experimental	Classic	Не	Discovered oscillatory phenomena in cryogenic piping.
Kramers et al. [4]	Analytical	-	He, N_2 , O_2	Derived linearized boundary layer theory. These equations require infinite temperature ratios for oscillations.
Trilling et al. [18]	Analytical	-	-	Derived sound pulses using linearized boundary layer theory in a tube heated on one end.
Clement et al. [19]	Experimental	Classic	Не	Documented changes in oscillations in different geometric configurations.
Bannister et al. [20]	Experimental	Classic	Не	Indicated a significant increase in convective heat transfer with oscillations.
Thurston et al. [21]	Experimental	Pipe flow	H_2	Recorded oscillations in hydrogen film boiling.
Rott et al. [3]	Analytical	-	Не	Derived fundamental thermoacoustic equations producing finite temperature ratios for oscillations.
Rott et al. [5]	Analytical	-	Не	Calculated the stability boundary for classical helium systems.
Von Hoffmann et al. [6]	Experimental	Classic	Не	Compared experimental data to Rott's predictions for the stability boundary.
Rott et al. [7]	Analytical	-	He, N ₂	Determined stability limits with tubes of varying cross-sections across the temperature profile.
Zouzoulas et al. [8]	Analytical	-	He, N ₂	Derived fundamental equations for gas-liquid oscillations in a tube. Calculated the stability limits for helium and nitrogen with gas-liquid interfaces.
Dmitrevskiy et al. [10]	Experimental	Classic	N_2 , Ar, O_2 , H_2	Measured oscillations as a function of tube height from the liquid interface.
Yazaki et al. [11]	Experimental	U-tube	He, Ne	Validated experimental stability boundaries with Rott's calculations.

Spradley et al. [12]	Experimental	Classic	Не	Characterized boil-off rates in helium dewars due to increased heat pumping with oscillations.
Collier et al. [22]	Experimental	-	H_2	Quantified oscillations in slush hydrogen systems as a function of fluctuating temperature.
Gu et al. [23]	Doctoral dissertation	Classic	He, H ₂	Measured oscillations in helium with a continuous temperature profile and compared results to theoretical model. Predicted stability boundaries for H ₂ systems.
Swift et al. [9]	Analytical	-	-	Expanded Rott's thermoacoustic theory for design of engines and refrigerators
Shimizu et al. [24]	Numerical (CFD)	Classic	Не	Proved relative variations in thermophysical parameters can affect mean values over time.
Shimizu et al. [25]	Numerical (CFD)	Classic	Не	Compared simulation calculations to Rott's stability boundaries and found good agreement but required lower temperature ratios than analytical calculations.
Ishigaki et al. [26]	Numerical (CFD)	U-tube	Не	Compared simulations to Rott's stability boundaries which predicted larger temperature ratios for excitation.
Sun et al. [27]	Numerical (CFD)	U-tube	H_2	Simulated oscillations in both axial and radial directions with hydrogen.
Putselyk et al. [14]	Empirical	-	-	Described numerous techniques for mitigation of oscillations in cryogenic storage vessels.
Luck et al. [15]	Analytical	Classic	-	Provided calculations to design additional damping reservoirs to mitigate oscillations.
Hu et al. [28]	Numerical (CFD)	Pipe flow	Не	Simulated oscillations in a pipeline of helium and discussed the mitigation of oscillations due to the installation of an adjustment tube.
Christie et al. [13]	Empirical	Classic	H_2	Discusses Taconis oscillations in practical cryogenic storage vessels and presents mitigation techniques.
Shenton et al. [29]	Experimental	U-tube	He, H ₂	Quantified oscillatory phenomena in U-shaped tube immersed in liquid nitrogen and validated two mitigation techniques.
Matveev [30]	Analytical	Classic	H_2	Predicted the onset of Taconis oscillations in a tube with compact resonators and porous inserts.

2. Experimentation

An experimental system has been designed and constructed to investigate Taconis oscillations in cryogenic hydrogen and helium systems and make comparisons with the thermoacoustic theory. Two different geometric configurations are explored, including a primarily constant-diameter tube and a system with wide cylindrical sections in the warm environment as they are more prone to Taconis phenomena.

2.1 Experimental Design

2.1.1 Cryostat and geometric configurations

A closed cryostat has been designed and constructed to investigate Taconis oscillations with cryogenic fluids (Figure 2). This system allows for cold temperature control, while regulating mean pressure inside the experimental tube. The cryostat utilizes a cryocooler operating at 60 Hz, which has a cooling capacity of approximately 20 W near 20 K, connected to the roof of the vacuum chamber. In addition, attached to the vacuum chamber, there are a dry scroll and turbo pump which can produce high vacuum pressures (10⁻⁶ Pascals). The specifics of design, construction, and performance of this cryostat are described by Shenton et al. [17].

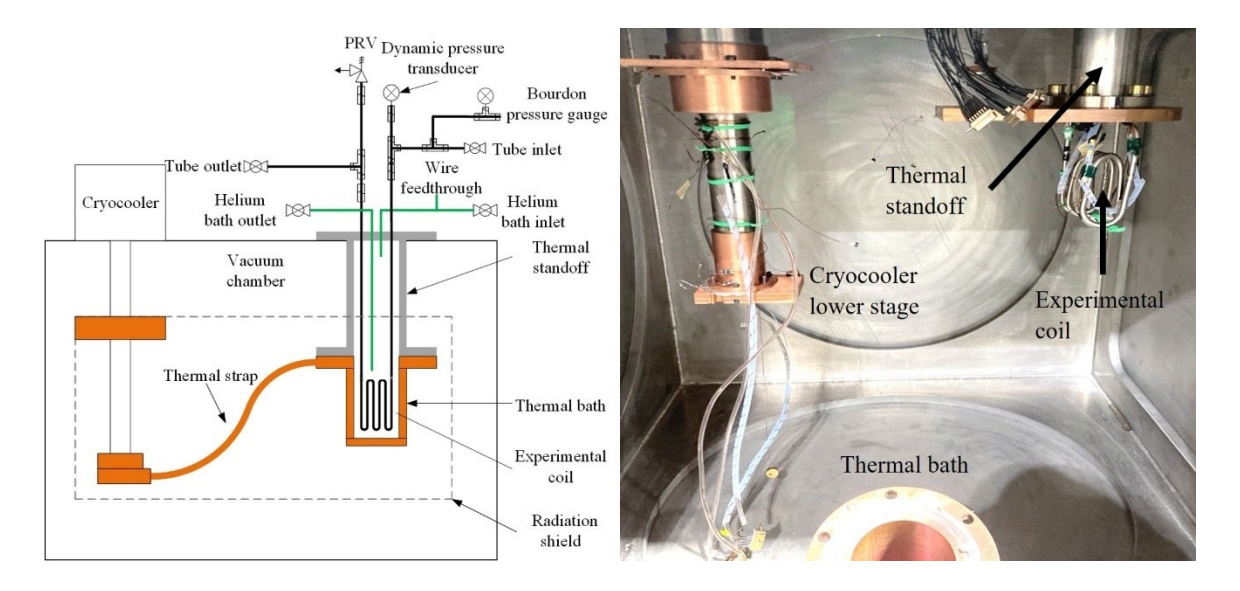


Figure 2. (a) System diagram of the experimental cryostat with U-shaped tube. (b) Photograph of the experimental setup being assembled. The thermal strap and radiation shield are not shown.

Inside the cryostat, a cylindrical copper test cell (thermal bath) is placed in a thermal dead end which contains helium. An experimental tube (made as a coil in the cold portion for compactness), filled with the working fluid (hydrogen or helium), is immersed in the helium thermal bath, which results in the temperature gradient from the ambient (outside the cryostat) and cryogenic (thermal bath) conditions. The 2nd stage of the cryocooler is connected to the thermal bath by a copper thermal strap (Figure 2a). A copper and multi-layered insulation (MLI) shield are wrapped around the experimental components to minimize radiative heat transfer from

the walls of the cryostat to the thermal bath. Temperature sensors are placed on the outside of the experimental tube and are connected to a wire feedthrough that is routed through the thermal bath inlet line.

Two geometric configurations are implemented in this study. The first configuration (Figure 3) uses a 6.35 mm outer diameter tube with wall thickness of 0.88 mm. The total length is 2.11 m. Short branches of the same tube are utilized to connect to other devices such as the inlet/outlet valves and a mean pressure gauge. These branches are connected to the main acoustic tube via SwagelokTM stainless steel 316 tee-fittings and unions. A pressure relief valve is connected to the top of the outlet side of the configuration. The experimental tube is routed through the roof of the cryostat using bore-through SwagelokTM fittings and is connected to the ambient tubing via SwagelokTM ultra-torr vacuum fittings.

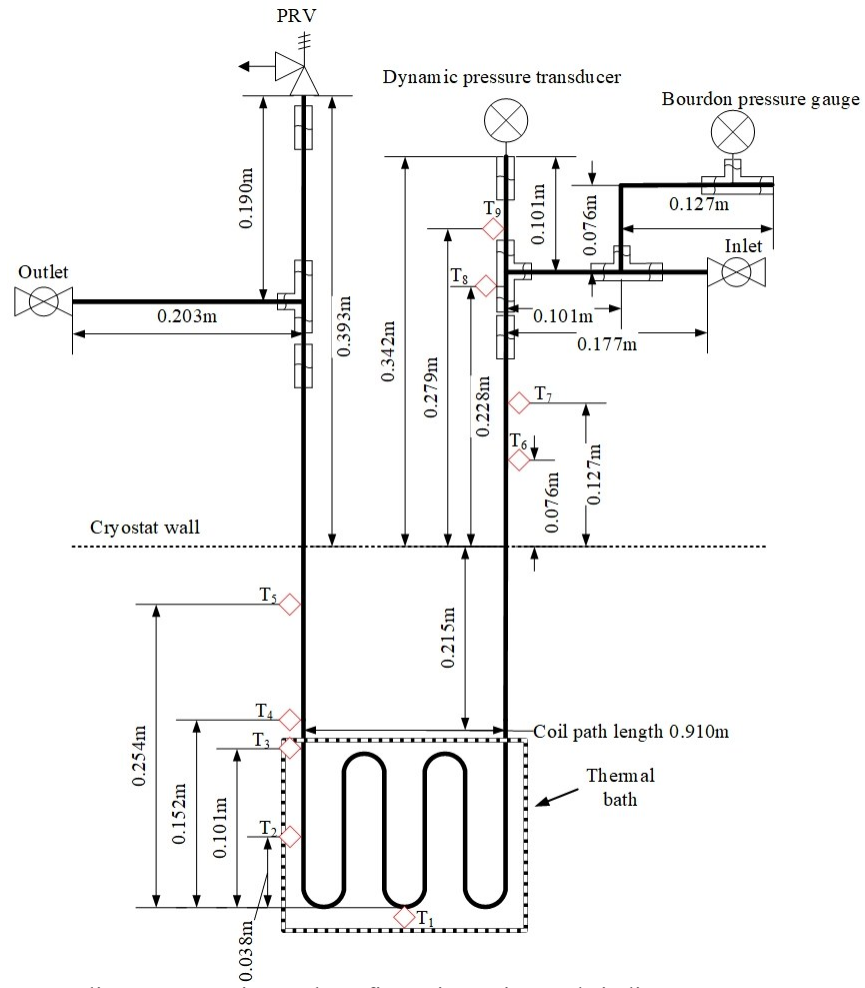


Figure 3. Constant-diameter experimental configuration. Diamonds indicate temperature sensor locations.

The second configuration uses the same 4.6 mm inner diameter tube for the cryogenic sections with consistent lengths. Since it is known that having a larger volume in ambient conditions excites oscillations at a smaller temperature gradient, larger diameter tubes are installed in the warm ambient environment with an internal diameter of 25.4 mm. This increased the overall length of the system by 0.88 m for a total length of 2.99 m.

The cryogenic section of tubing is wrapped into a coil to fit the dimensional constraints of the copper test cell with the thermal bath. The bend radius of the coil is equal to approximately

2 cm. Five temperature sensors are placed along the cryogenic portion of tubing to measure the temperature variation associated with the transition and thermal bath regions. The cryogenic temperature sensors are soldered to the stainless-steel tube using indium. The diamonds in Figure 3 and Figure 4 depict placements of these sensors. The length of tubing between sensors 3 and 4 corresponds to the connection plate between the thermal strap and the copper test cell.

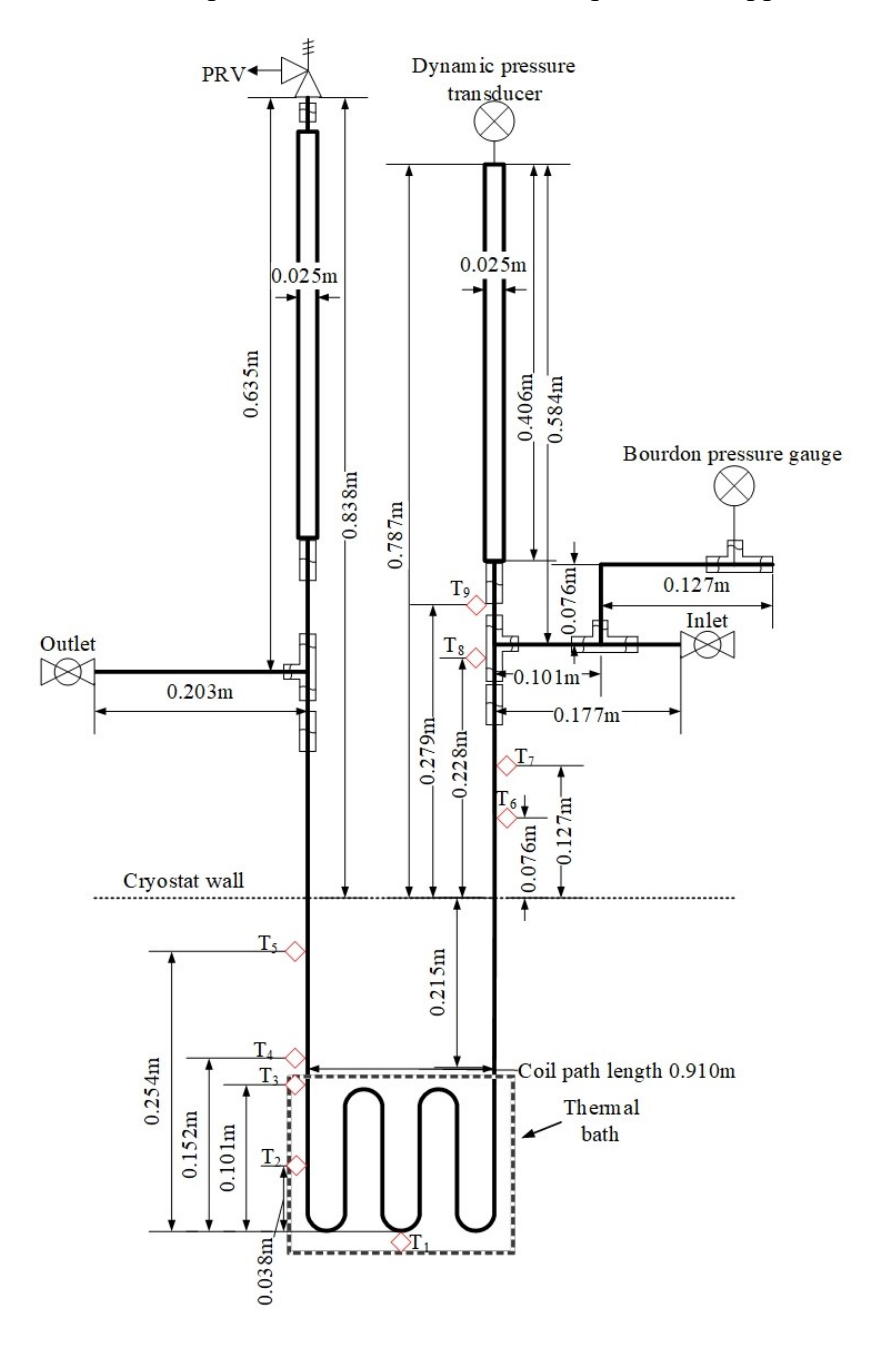


Figure 4. Variable-diameter experimental configuration. Diamonds indicate temperature sensor locations.

2.1.2 Instrumentation

The instrumentation for measuring the acoustic pressure, frequency, and temperature profiles is summarized in Table 2. Silicon diodes are used as temperature sensors (Figure 3 and Figure 4) with sensor 2, 4 and 5 acquired from Scientific InstrumentsTM with an uncertainty equal to ± 0.5 K and sensors 1 and 3 from LakeshoreTM with an uncertainty of ± 0.3 K. In addition, four OmegaTM type K thermocouples (sensors 6-9) are placed on the tubing outside of the cryostat to measure the changes to the ambient environment with an error of ± 1 K. The thermocouples are attached using mylar adhesive tape and recorded using an OmegaTM datalogger.

A PCBTM model 11b321 dynamic pressure transducer with an accuracy of $\pm 1\%$ records the acoustic pressure oscillations at one of the warm ends of the experimental tubing. The mean pressure is measured via a bourdon tube gauge with an error consisting of $\pm 3\%$ with a range equal to 2.8 MPa (gauge). Two 50 W cartridge heaters and external power supplies are used to control the heat applied to the system to maintain a desired cold temperature. One heater is connected directly to the 2^{nd} stage of the cryocooler. The other heater is installed at the top of the thermal bath.

Measurement	Instrument	Manufacturer	Uncertainty
Temperature	Silicon diode 415	Scientific Instruments TM	±0.5 K
Temperature	Silicon diode DT-670	Lakeshore TM	$\pm 0.3~K$
Temperature	Type K thermocouples	Omega TM	$\pm 1~K$
Acoustic Pressure	11b321	PCB^{TM}	1% absolute
Mean Pressure	400 psig	Matheson	±3% full scale

Table 2. Instrumentation used in experimental studies.

2.2 Experimental processes

Each experimental study started with achieving the desired mean pressure of the system with a certain ΔT , and consisted of manipulating the temperature of the thermal bath (affecting the cold tube temperature) to induce Taconis oscillations. The recorded data consists of the acoustic pressure, frequency, and temperature profile of the system. A LabviewTM program is created using the *Tone Measurements* library [31, 32] to determine the acoustic pressure and dominant frequency using a Fast Fourier Transform; and initial measurements were verified using MatlabTM. To regulate pressure in the system with a working fluid, inlet and outlet valves are utilized (shown in Figure 2a).

The inlet valves on the top of the system are open allowing gas to enter the tube. Ultrahigh purity (99.999%) helium and hydrogen are sourced from A-L Compressed GasesTM and NORCOTM respectively. The working fluid is regulated to the desired pressure from gaseous cylinders connected to the system. The thermal bath is pressurized (helium bath inlet valve) with helium at 299 kPa (30 psig). This pressure is held constant for all experimental runs. The experimental tube is pressurized using the tube inlet valve. Both valves are kept open during cool down of the system to allow mass to transfer into the system as densification of the gas occurs. Independent bourdon gauges measure the mean pressures in both the thermal bath and experimental tube. The outlet valves (nominally closed) allow for regulating pressure during expansion of the gas, and to have access to the vent line. The tube inlet valve is closed to create a

close-ended configuration once a desired pressure is reached in the coil for the experimental test. The mean pressure is kept constant during a test by adjusting the tube inlet and outlet valves between measurements.

The temperature profile of the system is adjusted using the cartridge heater connected to the thermal bath. A power supply introduces a constant amperage, and the voltage is measured in a 4-lead arrangement described in Ekin et al. [33]. Varying the amperage of the cartridge heater modifies the thermal bath temperature. The specific procedures for the different experimental studies are described in Section 4 which were conducted at a variety of mean pressures for helium and hydrogen.

3. Theoretical analysis

3.1 Governing thermoacoustic equations

Figure 5 schematically depicts a setup used for the theoretical modeling to estimate the cold onset temperature and onset frequency of Taconis oscillations. The system represents a narrow tube with higher temperature regions near the closed ends and a cold section in the middle portion of the tube. The low-amplitude thermoacoustic theory [9] is applied for modeling the system excitation under the following assumptions:

- 1) Quasi-1-D acoustic pressure and volumetric velocity undergo harmonic oscillations when the system is excited.
- 2) The governing thermoacoustic equations are derived using the ideal-gas approximation (but real fluid properties are used for mean values).
- 3) No mean volumetric velocity is present in the system.
- 4) Temperature fluctuations in the tube wall are ignored.

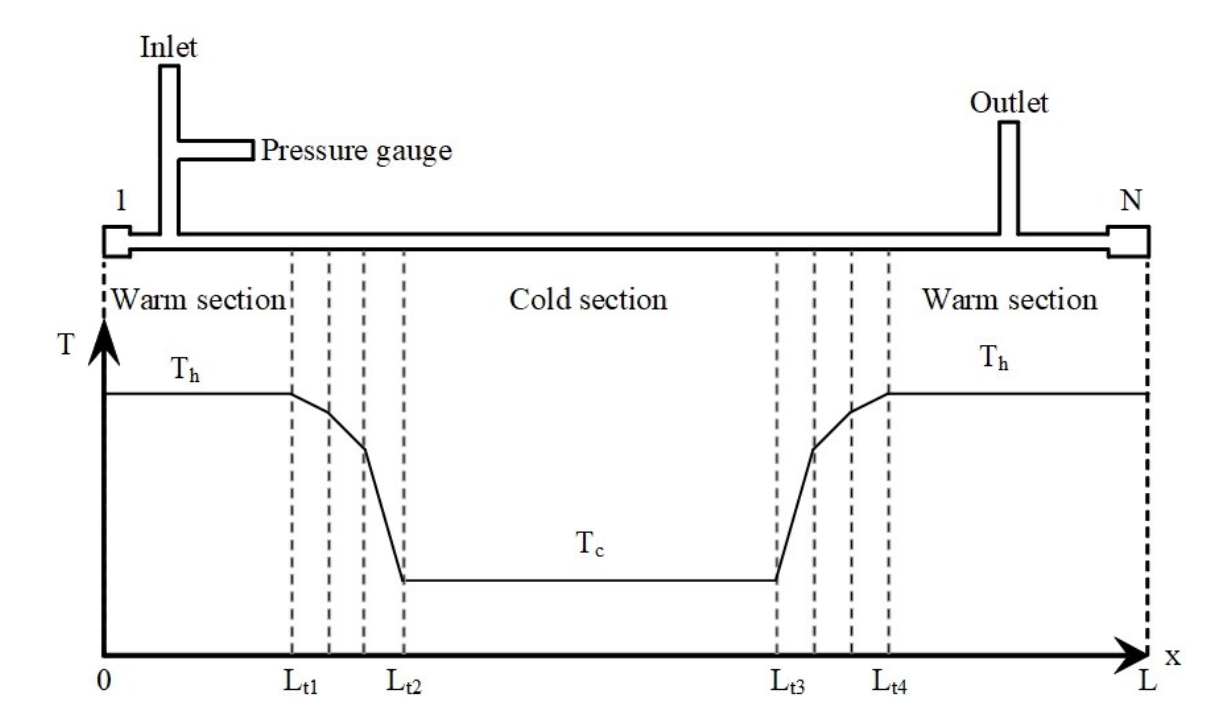


Figure 5. Representation (not to scale) of experimental system with axial temperature profile.

In the employed model, the oscillatory component of pressure (p') and the volumetric flow rate (U') are expressed with help of complex amplitudes (commonly used in acoustics), while the actual pressure and velocity fluctuations are given by the real parts,

$$p'(x,t) = Re[p(x)e^{i\omega t}],$$

$$U'(x,t) = Re[U(x)e^{i\omega t}],$$
(1)

$$U'(x,t) = Re[U(x)e^{i\omega t}], \tag{2}$$

where x is the coordinate along the tube, t is the time, i is the imaginary unity, ω is the angular frequency, and p and U are the complex amplitudes of the acoustic pressure and volumetric velocity, respectively. When considering steady-state single-frequency oscillations, the complex notation for the acoustic amplitudes allows for the transformation of the governing partial differential equations into ordinary differential equations by eliminating the time derivative.

The governing fluid mechanics equations can be linearized for low-amplitude acoustic oscillations, and the resulting equations for the acoustic amplitudes are reduced to one dimension in Rott's approximation [8],

$$dp = -\frac{i\rho_m \omega dx}{A_c (1 - f_v)} U,\tag{3}$$

$$dU = -\frac{i\omega A_c dx}{\gamma p_m} [1 + (\gamma - 1)f_k] p + \frac{f_k - f_v}{(1 - f_v)(1 - \sigma)} \frac{dT_m}{T_m} U,$$
(4)

where ρ_m , p_m and T_m are the mean (cross-section averaged) density, pressure, and temperature in the fluid, γ is the ratio of specific heats, and $\sigma = \frac{\mu c_p}{k}$ is the Prandtl number. Parameters μ , c_p and k are the viscosity, specific heat, and thermal conductivity of the fluid inside the tube, with A_c being the cross-sectional area [22].

The thermoacoustic functions f_k and f_v in Eqs. (3,4) depend on the channel geometry. For circular tubes they are given as follows [22],

$$f_{k,v} = 2 \frac{J_1(y_{k,v})}{y_{k,v}J_0(y_{k,v})},\tag{5}$$

$$y_{k,v} = \frac{(i-1)R}{\delta_{k,v}},\tag{6}$$

$$\delta_k = \sqrt{\frac{2k}{\rho\omega c_p}},\tag{7}$$

$$\delta_v = \sqrt{\frac{2\mu}{\rho\omega}},\tag{8}$$

where J_1 and J_0 are Bessel functions of the first and zero order, respectively, R is the tube radius, and δ_k and δ_v are the thermal and viscous penetration depths.

Equations (3-4) can also be utilized to characterize a conventional acoustic wave in an isothermal tube when the second term in Eq. (4) is zero. In tube sections with a temperature gradient, the second term results in either production of acoustic power from thermal energy or dissipation of acoustic power. In the present approach, these equations are discretized at N points along the tube,

$$U_{j+1} - U_j = -\frac{i\omega A_c dx}{\gamma P_m} \left[1 + (\gamma - 1)f_k \right] \left(\frac{p_{j+1} + p_j}{2} \right) + \frac{f_k - f_v}{(1 - f_v)(1 - \sigma)} \left(\frac{dT_m}{T_m} \right) \left(\frac{U_{j+1} + U_j}{2} \right), \tag{9}$$

$$p_{j+1} - p_j = -\frac{i\omega \rho_m dx}{A_c (1 - f_v)} \left(\frac{U_{j+1} + U_j}{2} \right), \tag{10}$$

where the thermophysical properties for the local functions $(f_{k,v})$ are taken at the average of the state points between each node.

The solution to this set of equations must also satisfy the boundary conditions associated with the setup shown in Figure 5. At point 1, placed at the tube end (x = 0), the tube is closed with a rigid surface dictating that the acoustic velocity must approach zero (ignoring a small variation through the penetration depth on this surface). At point N placed at the opposite end, the tube is also closed, creating another near-zero velocity requirement. These boundary conditions are expressed as the following:

$$U_1 = 0,$$
 (11)
 $U_N = 0.$ (12)

$$U_N = 0. (12)$$

For more complicated piping networks, involving branches connected to the main line (Figure 6), the following simplifying equations can be utilized at the junctions to ensure continuity between the main tube and the connection,

$$p_1 = p_2 = p_3, (13)$$

$$u_1 A_1 = u_2 A_2 + u_3 A_3. (14)$$

Using the low-amplitude approximation, the acoustic pressures are assumed to be constant at the junction and the volumetric acoustic velocity is conserved as shown in Eqs. (13-14). Added-masses, dissipative mechanisms, and other effects at junctions are neglected in this study.

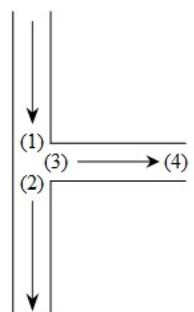


Figure 6. T-connection from the main tube network. Arrows define positive acoustic velocity.

If the branches are isothermal, then the analytical solutions to the conservation equations can be utilized to calculate the impedance associated with the branch. For example, if the branch is a constant diameter tube with area A_3 , acoustic amplitudes at two ends of this branch can be related as follows,

$$p_3 = \cos(kL_3) p_4 + \frac{i\rho_m c}{A_3} \sin(kL_3) U_4, \tag{15}$$

$$U_3 = \frac{iA_3}{\rho_m c} \sin(kL_3) p_4 + \cos(kL_3) U_4, \tag{16}$$

$$k = \frac{\omega}{c} \sqrt{\frac{1 + (\gamma - 1)f_k}{1 - f_v}},\tag{17}$$

where L_3 is the length of the branch, k is the wave number accounting for dissipation through the segment, and c is the sound speed taken at the isothermal temperature. If the branch ends at the length L_3 , volumetric velocity U_4 in Eqs. (15,16) will be zero.

To account for isothermal branches, one can calculate their acoustic impedances Z_{br} using the acoustic amplitudes at the entrance, p_{br} and U_{br} , and then correct the discretized thermoacoustic equations, assuming the branch is positioned between nodes i and i + 1,

$$Z_{br} = \frac{p_{br}}{U_{br}},\tag{18}$$

$$U_{j+1} - \left(U_j - \frac{p_j}{Z}\right) = -\frac{i\omega A_c dx}{\gamma P_m} \left[1 + (\gamma - 1)f_k\right] \left(\frac{p_{j+1} - p_j}{2}\right) + \frac{f_k - f_v}{(1 - f_v)(1 - \sigma)} \left(\frac{dT_m}{T_m}\right) \left(\frac{U_{j+1} + \left(U_j - \frac{p_j}{Z_{br}}\right)}{2}\right), (19)$$

$$p_{j+1} - p_j = -\frac{i\omega \rho_m dx}{A_c (1 - f_v)} \left(\frac{\left(U_{j+1} + \left(U_j - \frac{p_j}{Z_{br}} \right) \right)}{2} \right). \tag{20}$$

This additional term with the branch impedance Z_{br} vanishes in the nodes where no branches are present, and these equations reduce to Eqs. (9-10).

3.2 Solutions of discretized thermoacoustic equations

A solution that defines the onset for Taconis oscillations is determined by calculating the transition from a stable state (no oscillations occur) to an unstable state (oscillations are present). As described above, a set of equations can be formed for all tube segments and associated boundary conditions. The steady-state solution with a real frequency represents an acoustic wave that neither grows nor attenuates in time, characterizing the onset of Taconis oscillations. This set of linear algebraic equations, assuming some frequency, can be expressed in the following form,

$$[A]\{x\} = \{b\},\tag{21}$$

where the matrix [A] is formed by coefficients from Eqs (19-20), and vector [x] consists of the acoustic pressure and velocity amplitudes at each node. The vector [b] is zero except for the first term, which corresponds to an arbitrarily selected finite pressure amplitude at the closed end. Results for acoustic amplitudes in the tube will simply scale with a selected boundary amplitude.

To calculate this solution, the temperature profile at each node along the length of the tube should be defined. In this analysis, a constant temperature gradient is assumed between positions of temperature sensors, and the temperature profile is calculated by interpolation between known temperatures at these points. The temperature profile is assumed to be symmetric about the midpoint of the tubing configuration. From the experimental data, it follows that the warm section of tubing is kept approximately constant near 300 K. Under this constraint, the

temperature profile along the tube in the model is adjusted proportionally to the change in the cold temperature with variation becoming less pronounced in warmer sections.

After the temperature values are generated for all nodes, the fluid properties are determined using the mean pressure of the system and the temperature at each node. In this study, the working fluids are hydrogen and helium. Their properties are taken from the NIST REFPROP database [34], where the thermophysical properties are calculated using the Leachman et al. [35] and Vega et al. [36] fundamental equations of state for hydrogen and helium, respectively. The transport properties of hydrogen were given by Muzny et al. [37] for viscosity and Assael et al. [38] for thermal conductivity. The viscosity and thermal conductivity of helium were specified by Arp et al. [39] and Hands et al. [40] respectively.

The linear set of equations (Eq. 21) is solved by iterating through a range of frequencies and cold temperatures, allowing the temperature profile to evolve, until the boundary conditions (Eqs. 11-12) are satisfied. The corresponding cold temperature and frequency are defined and reported as the onset of Taconis oscillations. These values are compared to the experimental measurements.

4. Experimental Studies

Four experimental studies are conducted to determine: (1) the oscillation onset characteristics at variable mean pressures for each configuration; (2) the acoustic amplitudes, frequencies, and temperature profiles of oscillations while oscillations are excited, including regimes with subcooled cold temperatures; (3) exploration of supercritical hydrogen excitation; and (4) sample transient measurements describing the evolution of the acoustic wave.

4.1 Temperature profiles

The experimental temperature profiles are recorded at different states during all measurement sets. Figure 7 depicts examples of the mean temperature profiles for both the constant-diameter and variable-diameter configurations as functions of the distance from one of the closed ends. The grey dotted lines represent linear profiles from ambient conditions to the cold thermal bath temperature to approximately determine the average temperature gradients in the transition regions. The two working fluids (helium and hydrogen) are shown at the same mean pressure of 299 kPa for a state with oscillations near the onset. The mean temperature variability between recorded warmer (non-excited) states and the coldest (most excited) states is small, as the focus was on the onset conditions, while the cryocooler capacity limited the lowest values. For both working fluids, the ambient environment stays approximately constant close to 300 K even when the cold temperature of the system is modified using the heater at the cold test cell.

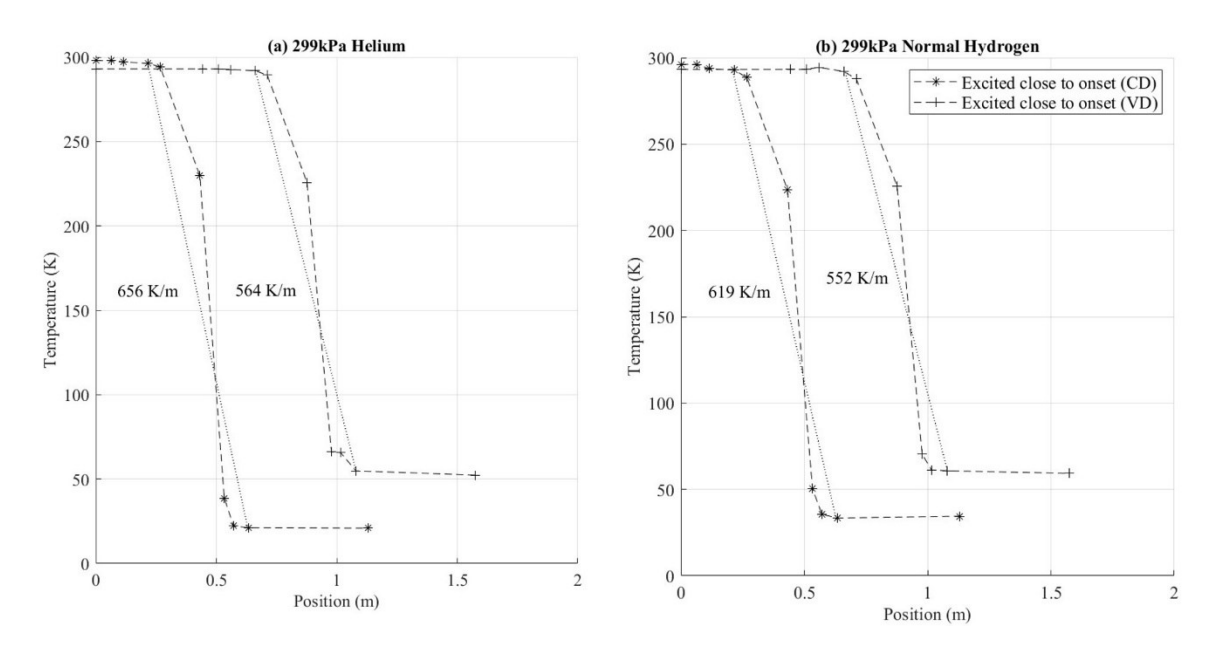


Figure 7. Temperature profiles (symbols connected by dashed lines) for each geometric configuration at 299 kPa with: (a) helium. (b) hydrogen. CD stands for constant-diameter and VD for variable-diameter tubes. Grey dotted lines show linear profiles from warm to cold regions with numbers indicating temperature gradients.

At 0.43 m down the tube (constant-diameter) and 0.88 m (variable-diameter) the temperature is about 230 K and varies approximately 1-2 K as the cold temperature is manipulated. In the cold section between 0.6 m-1.2 m in the constant-diameter (CD) configuration, the temperature remains almost constant along the tube within the uncertainty of the measurement. The cold temperature can be changed by ± 2 K relative to the onset profile shown in Figure 7 by changing heat supply to the test cell. The temperature profile in the variable diameter (VD) configuration with hydrogen in the cryogenic region (1 m-1.6 m) is also constant within the experimental uncertainty. However, with helium there is a small change in temperature of approximately 4 K which could be attributed to heat propagation down the tube when oscillations are present. The difference between helium and hydrogen is approximately 10 K for both geometric configurations as lower cold temperatures are needed to excite these setups with helium. The temperature gradients for hydrogen in both configurations are smaller than for helium (Figure 7). In the constant-diameter study, the temperature gradient is 619 K/m for hydrogen compared to 656 K/m for helium. The temperature gradient required for hydrogen excitation in the variable diameter setup is 552 K/m compared to 564 K/m with helium. The temperature gradients needed for excitation in the variable diameter configuration are also consistently lower than in the constant-diameter configuration, as wider tube sections in the warm part of the tube allowed for Taconis oscillations at higher cold temperature.

For presenting results in the following sections, the cold temperature is employed as the main variable parameter, since it was varied during the tests, whereas the warm temperature remained near 300 K. Another common temperature-related parameter used in the literature on Taconis oscillations is the ratio between warm and cold temperatures, which can be evaluated for the present data using the cold temperatures reported below and the approximately constant warm temperature.

4.2 Onset characteristics of hydrogen and helium

4.2.1 Stability boundaries

The acoustic pressure amplitude and frequency serve as the metrics characterizing the onset of oscillations and the excited regimes. Three measurement sets with varying cold temperatures are obtained and plotted at various mean pressures. The stability boundaries depict the transition from unexcited to excited oscillatory systems and are determined by incrementally changing the cold temperature using the cartridge heater connected to the thermal bath. An experimental study begins when a large temperature difference is established between the ambient environment and the cryogenic environment, due to the thermal bath, with the tube inlet valve open. The temperature gradient is set at the largest ΔT (between the ambient and cold zones) that the system can produce. With the tube inlet valve open, no oscillations are present in the system even with the large temperature gradient. The following steps are completed 3 times to determine the onset characteristics at a specific mean pressure.

- 1) The experimental tube is pressurized to the desired mean pressure for the study.
 - With hydrogen as the working fluid, the thermal bath temperature is adjusted (via the cartridge heater) so that the cold temperature of the tube is kept above the saturation temperature at the given pressure to ensure no liquid is present in the tube at the start of the study.
- 2) After pressurization, the tube inlet valve is closed.
 - When the tube inlet valve is closed, oscillations are excited in the tube if the temperature gradient is sufficiently large.
- 3) The temperature profile, acoustic pressure amplitude, and dominant frequency in the signal are continuously recorded.
- 4) The power supplied to the cartridge heater mounted to the thermal bath is increased in small increments (0.4 W), which raises the cold thermal bath temperature.
 - -The change from an excited system to a nonexcited system is established when the pressure fluctuations fall within the noise level, comparable with the transducer uncertainty. The temperature where this transition occurs is defined as a cold onset temperature.
- 5) The power supplied to the thermal bath is continually increased until the thermal bath temperature is approximately 2 K above the observed onset temperature where the pressure amplitude disappears.
- 6) The temperature of the thermal bath is decreased again by reducing the power supplied by the cartridge heater to re-establish the oscillations.
 - -The system is excited when the pressure transducer records an increase of a pressure amplitude above the noise level. The temperature, when the system becomes excited again, is also defined as a cold onset temperature for the system. These two cold onset temperatures may vary from each other due to possible hysteresis in the excitation of thermoacoustic oscillations. However, as shown in the results, this variation was within the uncertainty of the measurement in the present system.
- 7) The temperature of the thermal bath decreases (via reduction in heater power) until returning to the initial temperature of the study.

Experimental measurements have been completed for a range of mean pressures from 126 kPa to 1816 kPa in both geometric configurations. Figure 8 depicts a comparison between helium and hydrogen for a subset of the experimental studies with two different mean pressures, 161 kPa and 299 kPa, in the constant diameter configuration. The measurements above the onset temperature are filtered for readability, as the recorded voltage was within the readability of the pressure transducer. These non-excited states are shown with an amplitude of 0 kPa and a frequency of 0 Hz. The acoustic pressure amplitude increases while reducing the cold temperature below the onset value, as thermal-to-acoustic energy conversion increases at larger temperature gradients in the system. However, the frequency reduces due to the speed of sound decreasing at colder temperatures. A limited span of temperatures is shown in figure 8 to demonstrate the onset temperature for each working fluid at the given mean pressure. For example, the onset temperature for helium at mean pressure 161 kPa is approximately 26.5-27 K and the oscillation frequency is 58 Hz (Figure 8a and 8c). For hydrogen at the same mean pressure, the onset temperature and frequency are approximately 39 K and 94 Hz, respectively (Figure 8b and 8d). At 299 kPa, the onset temperature (Figure 8e) with helium decreases to approximately 21 K and the onset frequency is close to 54 Hz (Figure 8g). The onset characteristics for hydrogen (Figure 8f) at 299 kPa also decrease with the onset temperature being 36 K and the onset frequency of 90 Hz (Figure 8h). The pressure amplitudes are recorded farther from the onset condition in the excited regime. Helium at a mean pressure of 161kPa reaches pressure amplitudes up to 4 kPa with a temperature near 20 K. At 299 kPa mean pressure, the amplitude of oscillations is approximately 2 kPa. As hydrogen approaches the saturation temperature for each mean pressure, the amplitude of oscillations grows to the maximum value. At 161 kPa mean pressure, the amplitude of oscillations for hydrogen is approximately 11 kPa, whereas at 299 kPa mean pressure, the amplitude is approximately 8 kPa.

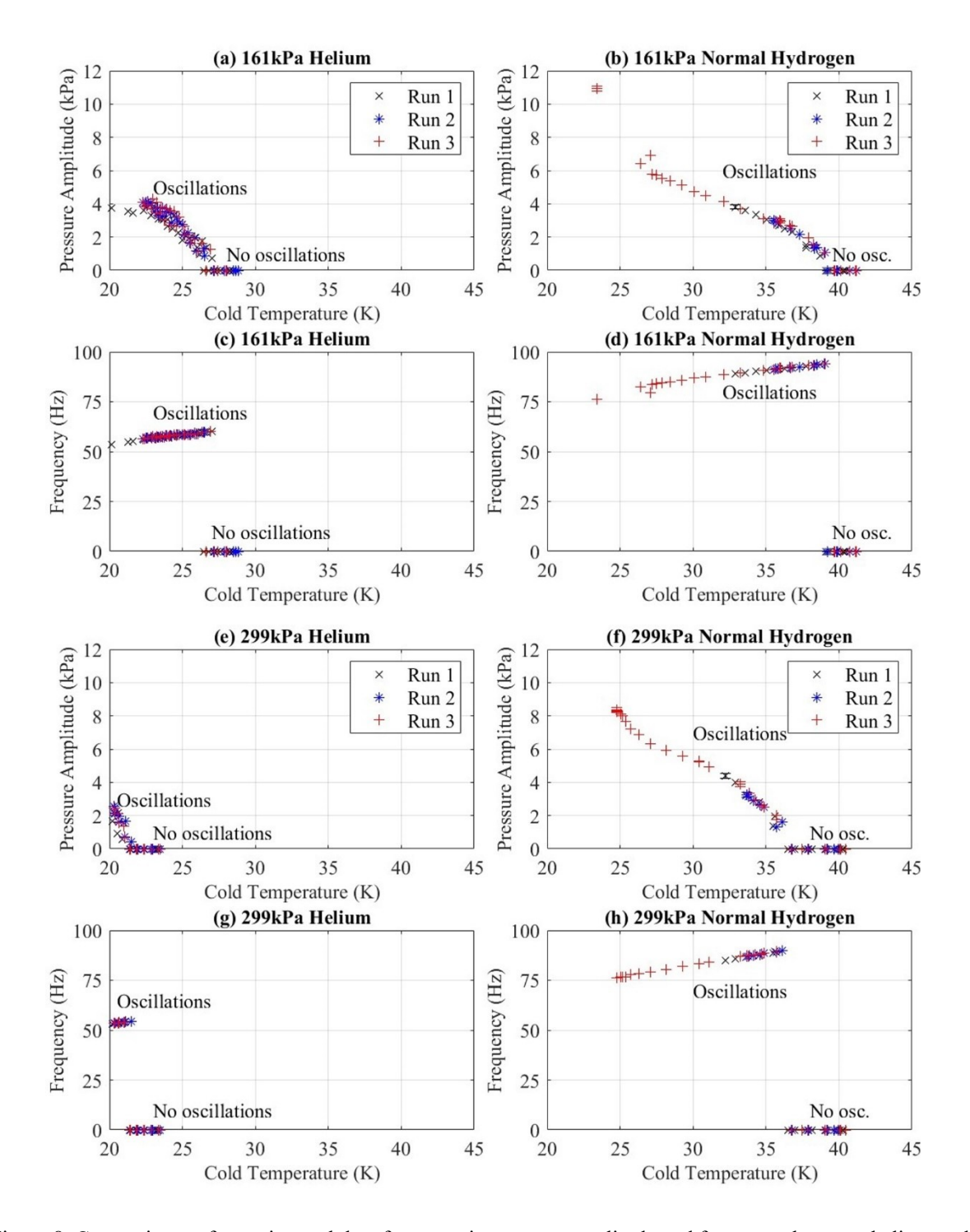


Figure 8. Comparisons of experimental data for acoustic pressure amplitude and frequency between helium and hydrogen in the constant-diameter configuration for: (a, c) 161 kPa helium, (b, d) 161 kPa normal hydrogen, (e, g) 299 kPa helium, (f, h) 299 kPa normal hydrogen.

The onset temperature in each geometric configuration is shown in the cold temperature-cold specific volume diagram for all studied conditions in Figure 9. As the error for these temperature measurements is about 0.7 K, the error bars are not included on the graph due to the small magnitude. The specific volume is calculated using the cold onset temperature and the mean pressure of the system. As the mean pressure increases for both helium and hydrogen in the constant-diameter setup, the cold onset temperature decreases. For helium, the decrease is approximately 10 K (from 30 K to 20 K) over the 200 kPa range. The onset temperature for hydrogen decreases with increasing pressure until 330 kPa. Above 330 kPa, the onset temperature is consistently near 35 K, which is still above the critical temperature. The onset temperatures drastically increase in the variable diameter setup. Helium shows similar trends with the onset temperature decreasing as mean pressure is increased, but at a smaller rate (5 K over a 1000 kPa span). The onset temperature in this configuration with hydrogen follows an opposite trend with a positive correlation between the mean pressure and the onset cold temperature. This range is on the order of 3 K. Hydrogen is consistently shown to excite easier than helium.

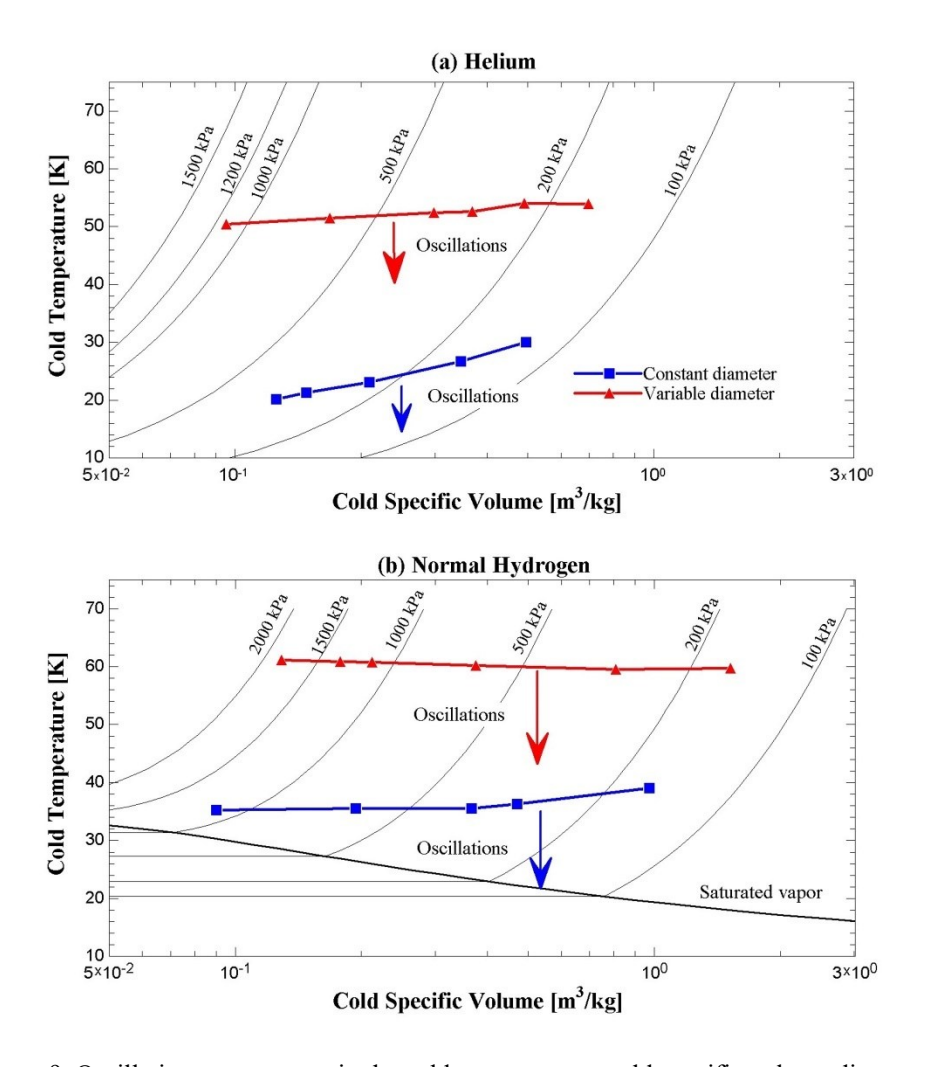


Figure 9. Oscillation onset curves in the cold temperature - cold specific volume diagram.

4.2.2 Comparison between experimental data and the thermoacoustic model

The experimental measurements obtained are compared to the calculations from the thermoacoustic model. Solutions for the acoustic pressure and volumetric flowrate are plotted along the position of the tube with onset conditions to verify the prediction method for the onset temperature and frequency. One example is shown in Figure 10 with hydrogen at a mean pressure of 299 kPa. The cold onset temperature is calculated as 29.2 K, and the frequency is 80 Hz. The acoustic pressure is evaluated with a value of 1% of the mean pressure at the rigid tube end. The maximum pressure amplitude occurs at the closed ends of the tubing, as shown in Figure 10a. The imaginary component is scaled by a factor of 10 for readability.

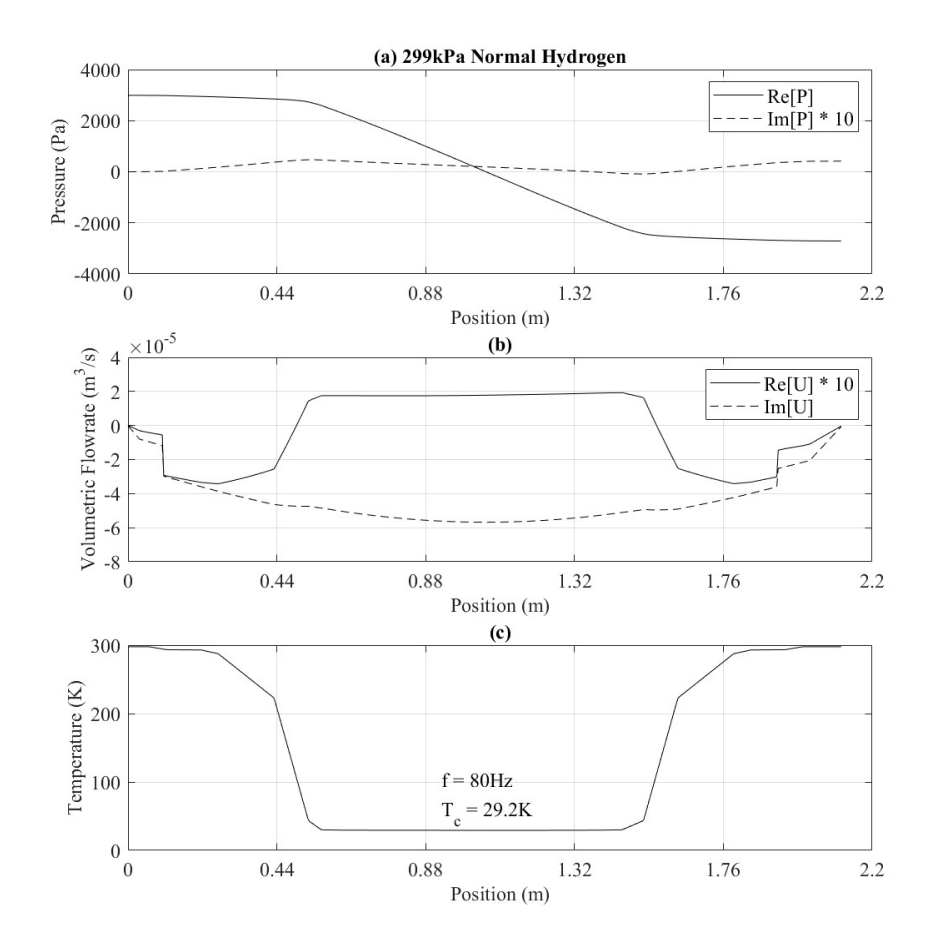


Figure 10. Solution profiles calculated at onset conditions for: (a) acoustic pressure. (b) volumetric flow rate. (c) temperature.

Figure 10b shows that the boundary conditions are satisfied as both the real and imaginary components of the volumetric flow rate approach zero at the closed ends of the main tube. The volumetric flow rate reaches a maximum at the center of the U-tube in the cryogenic region where there is an acoustic pressure node. These profiles lack exact symmetry and exhibit jumps in warm sections due to the additional branches connected to the main tube (Figures 3 and 4). The inlet branches have a smaller magnitude for volumetric flow rate than the outlet branch near the main tube ends. The volumetric flow rate increases after the inlet branch and decreases after the outlet branch. The results for the real component of the velocity are also scaled by a

factor of 10 for readability. The corresponding onset temperature profile is depicted in Figure 10c. This profile provides the temperatures to calculate the onset acoustic solutions.

The experimental onset characteristics are compared to thermoacoustic theory predictions in Figure 11 for both the constant- and variable- diameter setups at all mean pressures. The markers represent experimental measurements, and the lines show model calculations. The experimental uncertainty for the temperature is ± 0.7 K and $\pm 3\%$ for mean pressure. The model shows reasonably close agreement with test data of the configuration with large volumes in the warm section for both the onset temperature (Figure 11a) and frequency (Figure 11b). The onset temperature is calculated within 5% of the experimental measurements and the onset frequency is within 10% for helium and hydrogen. There is larger disagreement with the constant-diameter configuration. For helium, the calculations are within 30% for the onset temperature and 10% for the onset frequency. The model generally estimates lower onset parameters than shown by the experimental measurements.

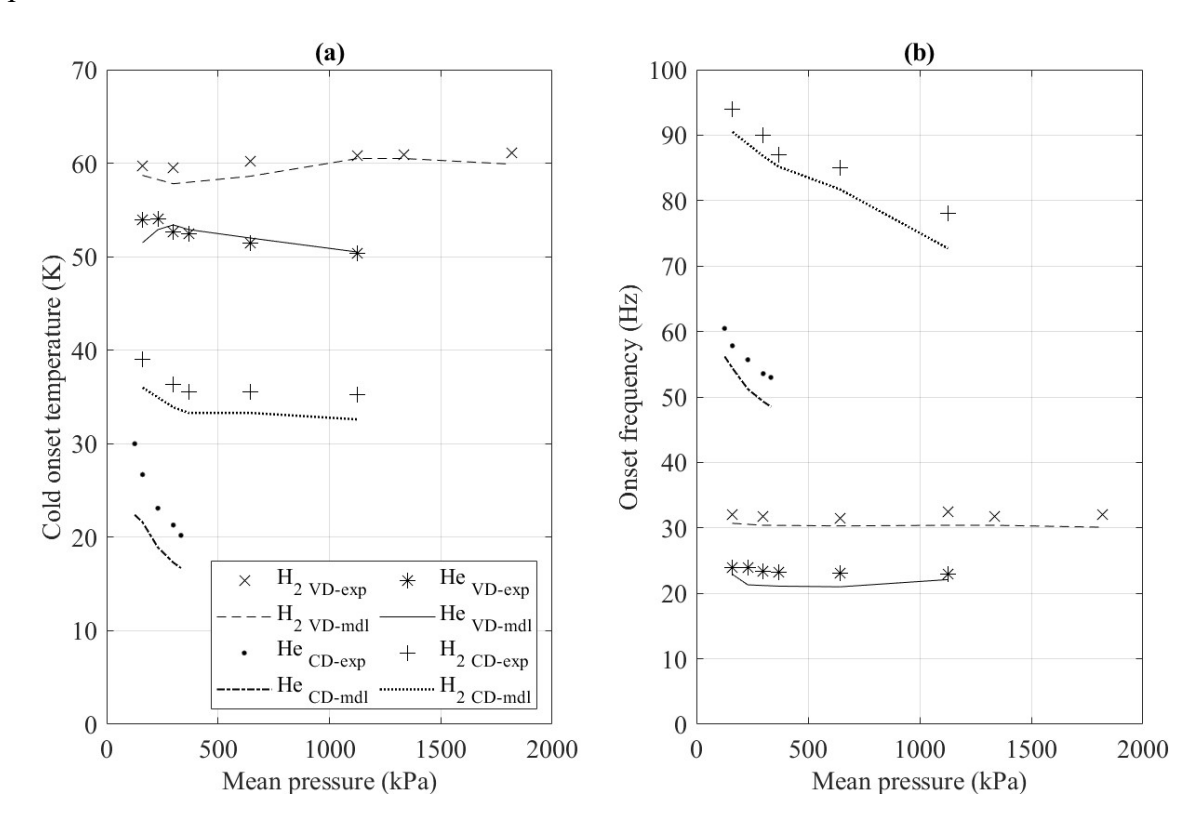


Figure 11. Comparison of experimental (exp) and modeling (mdl) onset characteristics: (a) onset temperature, (b) onset frequency. CD stands for the constant-diameter configuration and VD for the variable-diameter configuration.

Hydrogen onset data in the constant-diameter configuration are within 10% and 10% for temperature and frequency, respectively. However, thermoacoustic theory calculates the onset parameters below the saturation temperature at 1126 kPa. Several factors could contribute to the observed divergences in the constant-diameter configuration. Hydrogen's compressibility factor ranges from 0.97 to 0.7 in the studied conditions (defined at the cold onset temperature and mean pressure), which indicates the importance of real-fluid effects, whereas the theory is based on the ideal-gas assumption. While helium can be considered ideal at these temperatures, some unaccounted features of the experimental apparatus may cause excitation at higher temperatures. The connections and fittings in the warm zone can help induce an earlier transition to the excited

state, similar to what occurs with having wider tube sections. Since acoustic properties of these elements are not well known, they have not been incorporated into the model. In the setup with wider tube segments, the added volumes were much larger than volumes in the fitting elements, so those connections did not significantly affect the prediction of the system excitation. In addition, the linear temperature profile is assumed between the sensor locations in the system when discretizing the temperature profile for modeling. However, the temperature profile can evolve differently between the sensors.

4.3 Oscillations with liquid and supercritical hydrogen

A subset of data was collected at higher mean pressures to quantify the amplitude and frequency of Taconis oscillations with liquid present in the tube by manipulating the thermal bath temperature below the saturation temperature to condense the hydrogen. The acoustic behavior is documented in Figure 12 with a mean pressure of 644 and 1127 kPa. The oscillations begin at approximately 35 K for both mean pressures. The thermal bath temperature is decreased below the saturation temperature by decreasing the heater mounted to the thermal bath in 0.4 W increments. The cold temperature is decreased until approximately 2 K below saturation. After the cartridge heater is increased in 0.4 W increments until the oscillations disappeared at a cold temperature greater than 35 K. The saturation temperature for the lower pressure is approximately 28 K, and the amplitude of oscillations increases to 7 kPa at the saturation line (Figure 12a). After the cold temperature decreases below the saturation temperature and liquid starts forming in the system, the frequency of the oscillations (Figure 12c) begins to decrease from about 75 Hz to 35 Hz. The amplitude also decreases from 7 kPa to 1 kPa. As the temperature increases from the lowest state above the saturation line, the frequency increases from about 40 Hz to 50 Hz and returns to approximately 80 Hz after the liquid is fully vaporized. The amplitude, however, is consistent at the lower value of 2 kPa until the liquid is fully vaporized. The change in frequency correlates with liquid formation in the experimental system, as a larger mass at the cold end decreases the frequency.

There is a difference in amplitude and frequency of oscillations at the same cold temperature. This could depend on the presence of a two-phase fluid in the tube. Decreasing the heater power on the thermal bath causes liquefaction of the gaseous fluid below the saturation temperature forming liquid droplets inside the experimental tube. Continuing to liquefy hydrogen in the tube decreases both frequency and amplitude. After starting to increase the bath temperature above saturation, vaporization occurs as the liquid slug oscillates in the tube resulting in different frequencies and amplitudes at the same cold bath temperature. These experiments portray hysteresis in oscillation parameters due to the two-phase mixture in the tube.

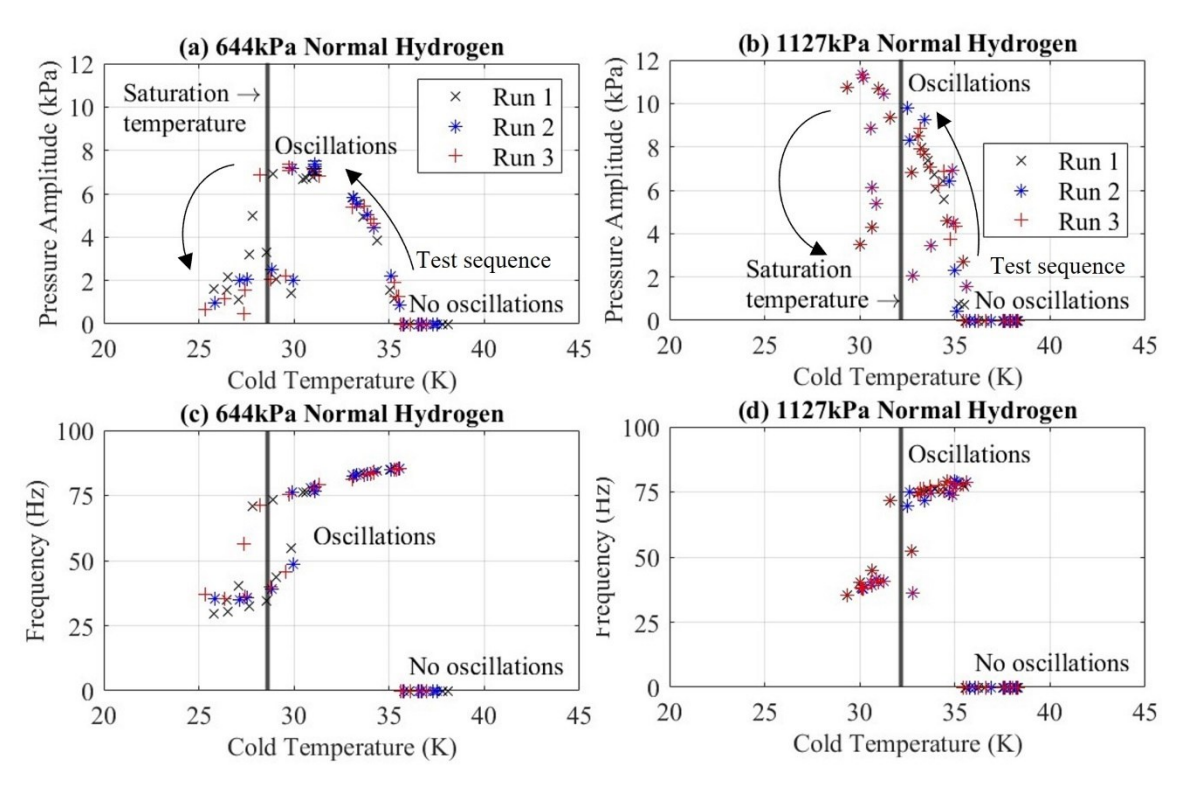


Figure 12. Taconis oscillations with liquid hydrogen at mean pressure: (a, c) 644 kPa, (b, d) 1127 kPa.

At 1127 kPa mean pressure, the oscillations are excited near 35 K and the pressure amplitude steadily increases to 11 kPa below the saturation line, and then decreases to approximately 4 kPa (Figure 12b). The frequency drops from 80 Hz to 40 Hz (Figure 12d). The amplitude does not return to 10 kPa until the liquid is vaporized in the tube. The frequency increases during the transition across the saturation line from about 40 to 70 Hz and finally back to 80 Hz. These experimental datapoints also show the differences in pressure amplitude and frequency at the same cold temperatures that can be associated with two-phase oscillatory flow. As the oscillations change due to liquid condensing in the tube, one may be curious if oscillations will change with supercritical hydrogen due to the different behavior of thermophysical properties above the critical point and no interfacial transition from a gaseous state to a liquid state. Another study is conducted to quantify the oscillation phenomena in supercritical hydrogen with results shown in Figure 13. The system is allowed to equilibrate above the critical temperature (33.1 K) for normal hydrogen by applying heat with the cartridge heater on the thermal bath. The mean pressure in the system is then set to 1816 kPa, and the inlet valve is closed. Oscillations become excited in the system. The external heat input is reduced in 0.4 W increments decreasing the cold temperature of the tube. Isobaric conditions are ensured by intermittently allowing mass transfer, via the tube inlet valve, into the closed system as densification occurs. The pressure amplitude, dominant frequency and temperature profile are recorded. The temperature in the system is decreased until the tube temperature is below the saturation temperature (24.7 K) for a mean pressure of 299 kPa. After that, the tube is depressurized to 299 kPa using the tube outlet valve. During depressurization, the oscillations attenuate as mass is vented out of the system. Once the tube outlet valve is closed, the oscillations re-excite. Then, heat input is added into the system (0.4 W increments) to raise the tube temperature back to the original state above the critical temperature. The coil outlet valve is

used to periodically vent hydrogen to maintain isobaric conditions as the fluid expands. The differences in frequency and pressure amplitude between the supercritical and subcritical gaseous hydrogen column are presented.

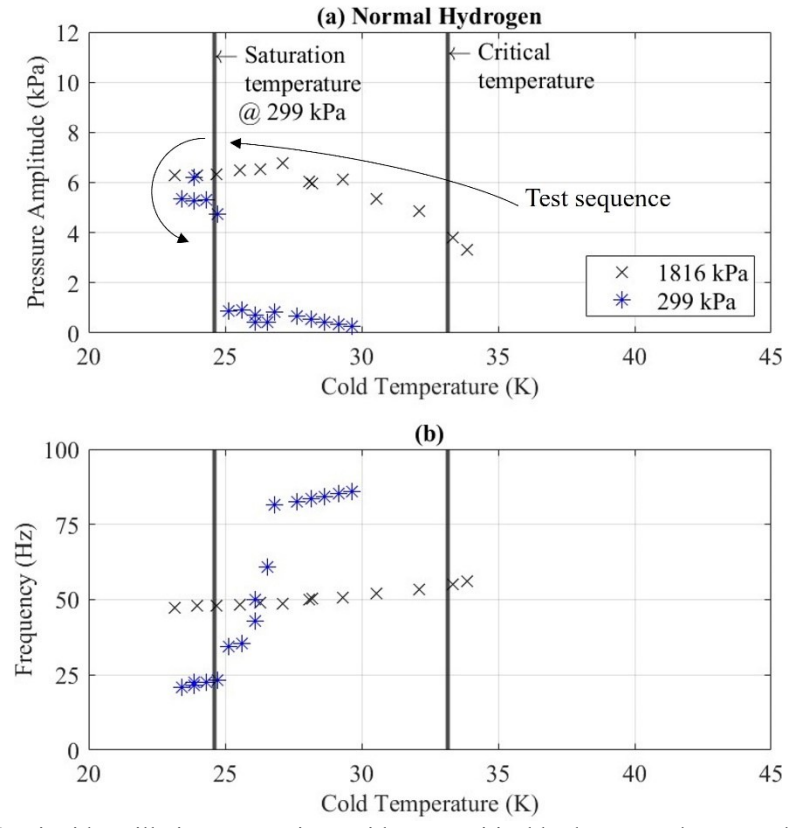


Figure 13. Liquid oscillation comparison with supercritical hydrogen and gaseous hydrogen.

The experimental coil pressurized to 1816 kPa shows oscillations with an amplitude of 4 kPa and a frequency of 58 Hz at an onset temperature near 34 K (just above the critical temperature). As the temperature decreases, the amplitude grows to approximately 7 kPa with a steady change in frequency down to about 47 Hz. The amplitude decreases to approximately 6 kPa below 24 K. The mean pressure is decreased to 299 kPa once the temperature is below the saturation line for 299 kPa. The oscillation parameters show trends similar to those in Figure 12. The frequency decreases to 20 Hz, and the amplitude is approximately 5 kPa. After the temperature increases above the saturation line, the amplitude drops to 1 kPa, and the frequency begins to increase to 80 Hz once the liquid is vaporized in the coil. The change in frequency and amplitude could be attributed to the formation of an interface between the gas and liquid inside the tube after reducing the mean pressure below the critical pressure. This study portrays Taconis oscillation characteristics (acoustic pressure and frequency) as path-dependent of hydrogen thermophysical and transport properties. There is a discrepancy between the amplitude of oscillations at a mean pressure of 299 kPa compared with previous experimental runs at isobaric conditions which could be due to the path dependency of the working fluid state.

4.4 Time-resolved excitation of Taconis oscillations

To provide sample information on the excitation dynamics, a few experiments were conducted to gather sample information on the time-resolved excitation process. The variable-diameter system was utilized for these studies as the experimental apparatus could reach temperatures of approximately 20 - 30 K below the onset temperature of oscillations. In these cases, the experimental system begins at thermal equilibrium at the coldest allowable temperature (above saturation temperature for hydrogen) with the tube valve open. Data recording starts prior to closing the inlet valve. Closing the valve immediately results in the appearance of oscillations. The temperature and acoustic pressure profiles are recorded for approximately one minute at several mean pressures. Different mean pressures are utilized for helium (161kPa and 1127 kPa) and hydrogen (299 kPa and 1127 kPa) with the variable-diameter system. The pressure oscillations evolve into a sinusoidal signal following the initial peak (Figure 14c). Using helium at 161 kPa, the pressure amplitude saturates at about 0.02 of the mean pressure. The temperatures along the tube increase as the heat load into the system increases due to convection associated with the oscillatory fluid motions caused by Taconis oscillations (Figure 14a). This results in a relatively large mean temperature increase of 10-20 K. When the mean pressure is 1127 kPa, more complex dynamic phenomena take place. Spikes in the wave occur, increasing the normalized pressure amplitude from a baseline 0.015 to about 0.02 and back. These beating phenomena repeat approximately every 10 seconds after the valves are closed (Figure 14d). The evolution of the temperature profile also reflects this phenomenon, with the temperature increase and decrease in time (Figure 14b) in the cryogenic section of tubing ranging over 5 K. Towards the warm section the temperature fluctuates by approximately 3 K.

Hydrogen data follow similar trends as in helium. At 299 kPa the sinusoidal wave develops to the normalized amplitude of approximately 0.01. The temperature profile increases in the cryogenic section and decreases in the warm section of tubing due to thermoacoustic heat transport (Figure 14e and g). When the mean pressure is 1127 kPa (Figure 14f, h), acoustic oscillations exhibit pulse-type behavior with the normalized amplitude fluctuating from 0.007 to 0.01 every 15 seconds, and this is accompanied by temperature fluctuations with magnitudes similar to those with helium. The observed dynamic phenomenon occurs in these studies only when the thermal bath temperature is well below the onset temperature for the system, the working fluid is in a gaseous phase, and with high mean pressures in the study. The variation in amplitude can be attributed to the rapid evolution in the temperature profile due to significant convective heat transfer caused by oscillatory flow. No attempt to model this behavior was made in this study, but similar patterns were predicted for start-up regimes of thermoacoustic engines operating on the same fundamental principles as Taconis oscillations [41].

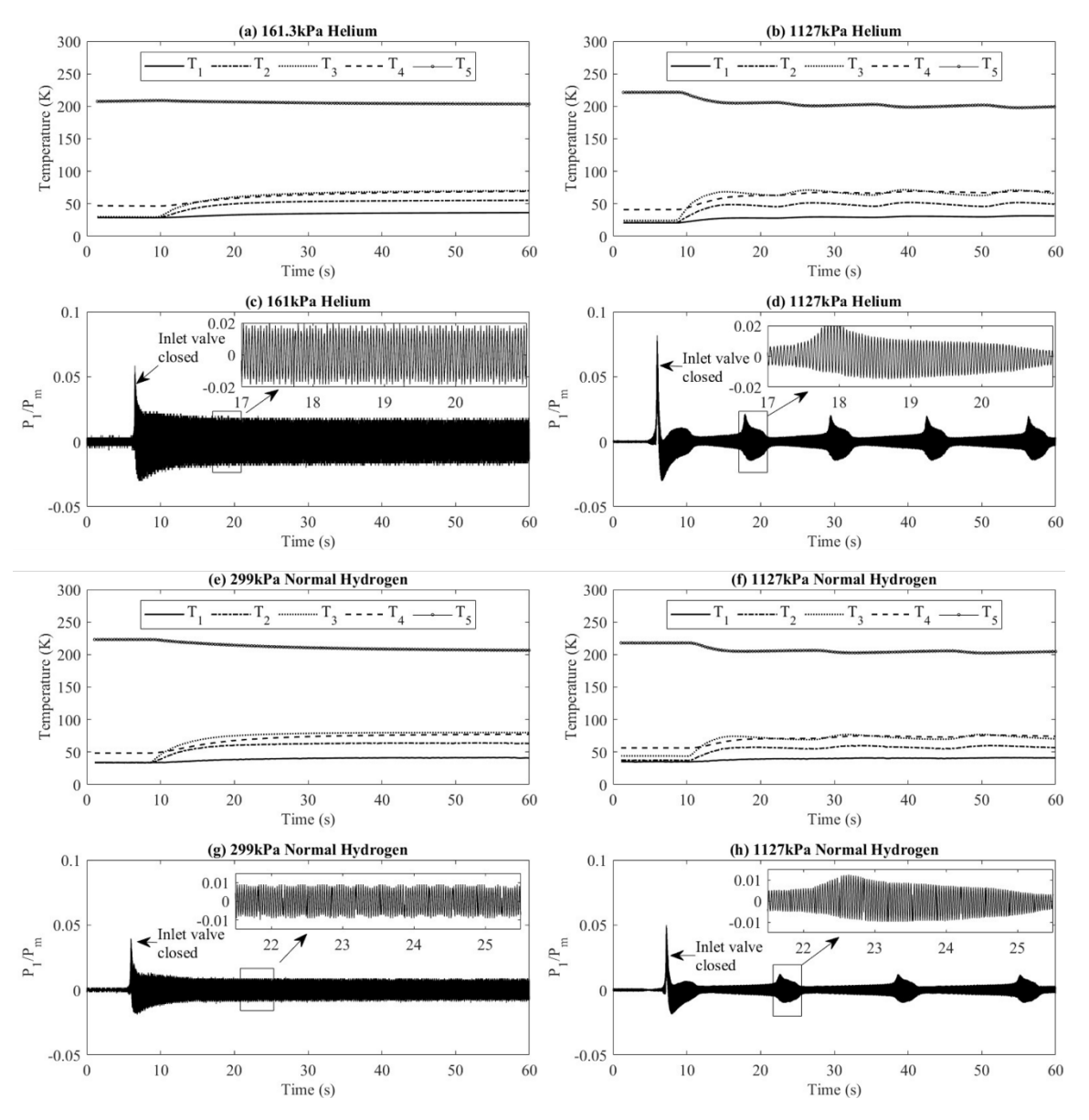


Figure 14. Temperature sensor readings and acoustic pressure below onset conditions in the variable-diameter system: (a-b) temperature profiles for 161 kPa and 1127 kPa helium, (c-d) normalized acoustic pressure for 161 kPa and 1127 kPa helium, (e-f) temperature profiles for 299 kPa and 1127 kPa normal hydrogen, (g-h) normalized acoustic pressure for 161 kPa and 1127 kPa normal hydrogen.

5. Conclusion

Taconis oscillations can increase boil-off rates and produce unwanted vibrations in cryogenic hydrogen storage tanks. Experimental measurements of the stability boundaries for hydrogen and helium were obtained to describe the onset temperatures and acoustic amplitudes and frequencies in a U-shaped tube between warm ambient and cold cryogenic environments. These measurements are compared against the low-amplitude thermoacoustic theory to validate the prediction of the onset parameters. The present experimental study shows that (1) hydrogen systems excite at smaller temperature gradients than those with helium; (2) tubing geometry affects when oscillations occur, and specifically, increasing the diameter of the tubing in the warm section decreases the temperature gradient required for excitation; and (3) increase of mean pressure generally reduces excitation. In addition to the stability boundaries at subcritical gaseous states, the Taconis oscillations are quantified in several two-phase and supercritical conditions. The frequency and amplitude of oscillations decrease when the cold temperature drops below saturation (i.e., when liquid appears). For supercritical hydrogen, the frequency is found to decrease, but the amplitude does not vary significantly compared to the subcritical gaseous state. Finally, dynamic phenomena are characterized in some conditions with the cold temperature below the onset value. As the mean pressure increases in the system, the acoustic amplitude spikes appear during the transition to the excited state, which lead to bursts of thermoacoustic heat transport into the cold region. The simplified thermoacoustic model showed a reasonable agreement for the onset of Taconis oscillations in the variable-diameter system. However, the model more substantially deviates from the experimental values in the constantdiameter setup. The unaccounted-for tube fittings and real fluid effects are some of the potential causes for this discrepancy.

Future research directions can include experimental studies of Taconis effects in broader parametric ranges, including different tube diameters, lengths, and various tube networks. On the modeling side, an attempt should be made to account for acoustic properties of tube fittings, relax the ideal-gas assumptions of the employed thermoacoustic theory, and include nonlinear and unsteady thermal analysis for the mean temperatures.

Acknowledgements

This research was supported in part by the U.S. National Science Foundation, grant number 2214235. We also extend our gratitude to Nathan P. Jorgensen for his help in the construction and maintenance of the cryostat and data collection.

References

- [1] Rayleigh JWSB. The theory of sound. United Kingdom: Macmillan; 1896.
- [2] Taconis K, Beenakker J, Nier AO, Aldrich L. Measurements Concerning the Vapor-Liquid Equilibrium of Solutions of He 3 in He 4 below 2.19 K. Physical Review. 1949;75(12):1966.
- [3] Rott N. Damped and thermally driven acoustic oscillations in wide and narrow tubes. Zeitschrift für angewandte Mathematik und Physik ZAMP. 1969;20:230-43.
- [4] Kramers H. Vibrations of a gas column. Physica. 1949;15(11-12):971-84.
- [5] Rott N. Thermally driven acoustic oscillations. Part II: Stability limit for helium. Zeitschrift für angewandte Mathematik und Physik ZAMP. 1973;24:54-72.
- [6] Von Hoffmann T, Lienert U, Quack H. Experiments on thermally driven gas oscillations. Cryogenics. 1973;13(8):490-2.
- [7] Rott N, Zouzoulas G. Thermally driven acoustic oscillations, part IV: tubes with variable cross-section. Zeitschrift für angewandte Mathematik und Physik ZAMP. 1976;27:197-224.
- [8] Zouzoulas G, Rott N. Thermally driven acoustic oscillations, part V: Gas-liquid oscillations. Zeitschrift für angewandte Mathematik und Physik ZAMP. 1976;27:325-34.
- [9] Swift GW. Thermoacoustics: A unifying perspective for some engines and refrigerators. Mellville, NY, USA: Acoustical society of America; 2003.
- [10] Dmitrevskiy YP, Mel'nik YM. Observation of thermal-acoustic oscillations in hydrogen, nitrogen, oxygen, and argon. Cryogenics. 1976;16(1):25-8.
- [11] Yazaki T, Tominaga A, Narahara Y. Experiments on thermally driven acoustic oscillations of gaseous helium. Journal of low temperature physics. 1980;41:45-60.
- [12] Spradley L, Dean W, Karu Z. Experimental and analytical study of thermal acoustic oscillations. NASA; 1975. Contract No.: LMSC-HREC TR D390690-II
- [13] Christie RJ, Hartwig JW. Thermal Acoustic Oscillation: Causes, Detection, Analysis, and Prevention. Thermal and Fluids Analysis Workshop 2014; Cleveland, Ohio 2014.
- [14] Putselyk S. Thermal Acoustic Oscillations: Short Review and Countermeasures. IOP Conference Series: Materials Science and Engineering; Hartford, Connecticut: IOP Publishing; 2020. p. 012080.
- [15] Luck H, Trepp C. Thermoacoustic oscillations in cryogenics. Part 3: avoiding and damping of oscillations. Cryogenics. 1992;32(8):703-6.
- [16] Keller W. Cryogenic Instrumentation at and above Liquid Hydrogen Temperature—Present and Future. Advances in Cryogenic Engineering: Proceedings of the 1972 Cryogenic Engineering Conference National Bureau of Standards Boulder, Colorado August 9–11, 1972: Springer; 1973. p. 289-300.
- [17] Shenton MP, Leachman JW, Matveev KI. Development of a research cryostat for direct thermoacoustic cooling and conversion of hydrogen. Cryogenic Engineering Conference; Honolulu, Hawaii. IOP Conference Series: Materials Science and Engineering: IOP Publishing; 2023. p. 012069.
- [18] Trilling L. On thermally induced sound fields. The Journal of the Acoustical Society of America. 1955;27(3):425-31.
- [19] Clement J, Gaffney J. Thermal oscillations in low temperature apparatus. Advances in Cryogenic Engineering: Proceedings of the 1954 Cryogenic Engineering Conference National Bureau of Standards Boulder, Colorado September 8–10 1954: Springer; 1960. p. 302-6.

- [20] Bannister J. Spontaneous Pressure Oscillations in Tubes Connecting Liquid Helium Reservoirs to [300° K Environments. Pure and Applied Cryogenics. 1966;6:127-35.
- [21] Thurston R, Rogers J, Skoglund V. Pressure oscillations induced by forced convection heating of dense hydrogen. Advances in Cryogenic Engineering: Proceedings of the 1966 Cryogenic Engineering Conference University of Colorado Engineering Research Center and Cryogenics Division NBS Institute for Materials Research Boulder, Colorado June 13–15, 1966: Springer; 1967. p. 438-51.
- [22] Collier R. Thermally induced oscillations in cryogenic systems. National Bureau of Standards; 1972. Contract No.: NBS-10-749.
- [23] Gu Y. Thermal acoustic oscillations in cryogenic systems [dissertation]: University of Colorado at Boulder; 1993.
- [24] Shimizu D, Sugimoto N. Numerical study of thermoacoustic Taconis oscillations. Journal of Applied Physics. 2010;107(3).
- [25] Shimizu D, Sugimoto N. Marginal conditions of thermoacoustic Taconis oscillations revisited. Proc of 20th International Congress on Acoustics, ICA; Sydney, Australia 2010.
- [26] Ishigaki M, Kuzuu K, Adachi S, Ishii K. Temperature Distribution in a Two-dimensional Closed Tube with Taconis Oscillation. Theoretical and Applied Mechanics Japan. 2009;57:351-62.
- [27] Sun D, Wang K, Guo Y, Zhang J, Xu Y, Zou J, et al. CFD study on Taconis thermoacoustic oscillation with cryogenic hydrogen as working gas. Cryogenics. 2016;75:38-46.
- [28] Hu L, Yang P, Chen P, Liu Y. Numerical study on suppression of thermoacoustic oscillation in cryogenic helium pipeline system. Cryogenics. 2021;117:103311.
- [29] Shenton MP, Matveev KI, Leachman JW. Initiation and suppression of Taconis oscillations in tubes with junctions, valves, and variable-diameter tube segments. Cryogenics Engineering Conference; Honolulu, Hawaii. IOP Conference Series: Materials Science and Engineering: IOP Publishing; 2024. p. 012042.
- [30] Matveev KI. Influence of Porous Inserts and Compact Resonators on Onset of Taconis Oscillations. Journal of Vibration and Acoustics. 2024;146(1).
- [31] Corporation NI. Tone Measurements: National Instruments; 2024 [Available from: https://www.ni.com/docs/en-US/bundle/labview-api-ref/page/vi-lib/express/express-analysis/toneblock-llb/ex-inst-tone-measurements-vi.html.
- [32] Corporation NI. LabVIEW Sound and Vibration Toolkit User Manual: National Instruments Corporation; 2004 [Available from: https://docsamples.wordpress.com/wp-content/uploads/2012/02/svt_um.pdf.
- [33] Ekin J. Experimental techniques for low-temperature measurements: cryostat design, material properties and superconductor critical-current testing. United Kingdom: Oxford university press; 2006.
- [34] E. W. Lemmon IHB, M. L. Huber, M. O. McLinden. NIST Standard Reference Database 23: Reference Fluid Thermodynamic and Transport Properties-REFPROP, Version 10.0, National Institute of Standards and Technology. 2018.
- [35] Leachman JW, Jacobsen RT, Penoncello SG, Lemmon EW. Fundamental Equations of State for Parahydrogen, Normal Hydrogen, and Orthohydrogen. Journal of Physical and Chemical Reference Data. 2009;38(3):721-48.
- [36] Vega DO, Hall K, Holste J, Harvey AH, Lemmon EW. An Equation of State for the Thermodynamic Properties of Helium. NIST Interagency/Internal Report (NISTIR) 8474 (National Institute of Standards and Technology); 2023.

- [37] Muzny CD, Huber ML, Kazakov AF. Correlation for the viscosity of normal hydrogen obtained from symbolic regression. Journal of Chemical & Engineering Data. 2013;58(4):969-79.
- [38] Assael MJ, Huber M, Perkins R, Takata Y. Correlation of the Thermal Conductivity of Normal and Parahydrogen from the Triple Point to 1000 K and up to 100 MPa. Journal of Physical and Chemical Reference Data. 2011;40(3).
- [39] Arp VD, McCarty RD. Thermophysical Properties of Helium-4 from 0.8 to 1500 K with Pressures to 2000 MPa. National Institute of Standards and Technology; 1998.
- [40] Hands B, Arp V. A correlation of thermal conductivity data for helium. Cryogenics. 1981;21(12):697-703.
- [41] Matveev KI. Unsteady model for standing-wave thermoacoustic engines. Journal of Non-Equilibrium Thermodynamics. 2010;35(2):85-96.